nature climate change

LETTERS

https://doi.org/10.1038/s41558-018-0263-1

Rapid coastal deoxygenation due to ocean circulation shift in the northwest Atlantic

Mariona Claret[1,2,3*], Eric D. Galbraith[3,4,5], Jaime B. Palter[6], Daniele Bianchi[7], Katja Fennel[8], Denis Gilbert[9] and John P. Dunne[10]

Global observations show that the ocean lost approximately 2% of its oxygen inventory over the past five decades[1–3], with important implications for marine ecosystems[4,5]. The rate of change varies regionally, with northwest Atlantic coastal waters showing a long-term drop[6,7] that vastly outpaces the global and North Atlantic basin mean deoxygenation rates[5,8]. However, past work has been unable to differentiate the role of large-scale climate forcing from that of local processes. Here, we use hydrographic evidence to show that a Labrador Current retreat is playing a key role in the deoxygenation on the northwest Atlantic shelf. A high-resolution global coupled climate–biogeochemistry model[9] reproduces the observed decline of saturation oxygen concentrations in the region, driven by a retreat of the equatorward-flowing Labrador Current and an associated shift towards more oxygen-poor subtropical waters on the shelf. The dynamical changes underlying the shift in shelf water properties are correlated with a slowdown in the simulated Atlantic Meridional Overturning Circulation (AMOC)[10]. Our results provide strong evidence that a major, centennial-scale change of the Labrador Current is underway, and highlight the potential for ocean dynamics to impact coastal deoxygenation over the coming century.

There is wide consensus that the global ocean oxygen (O_2) concentration is decreasing, and will continue to do so over the next century due to global warming[11,12]. Thus far, the O_2 inventory of the North Atlantic basin has not followed the general trend[2], but has instead shown a marked spatial variability driven by natural climate oscillations[13,14] that approximately balance over the whole basin[15]. However, despite the muted historical change for the North Atlantic on average, dramatic long-term deoxygenation trends have been reported over the past century on the northwest Atlantic shelf[6,7,16] (Fig. 1), a region that hosts a highly productive benthic ecosystem.

The recent deoxygenation trends are also recorded in marine sediments in the region[17,18], where they stand out as unique occurrences over the past millennium, and palaeoceanographic records document warming, salinification and changing nutrient supply on the Scotian Shelf during the past century[19–21]. It has been speculated that these coastal changes reflect variations in the large-scale offshore circulation that involves the Gulf Stream, which transports oxygen-poor tropical and subtropical water masses northwards, and the Labrador Current, which transports well-oxygenated water masses southwards[7,20]. However, it has been difficult to piece together the observations given their sparsity, and both the ocean dynamics and biogeochemistry in this complex region are not well represented by the coarse resolution typical of global climate models[22–24], which leaves the underlying mechanisms poorly understood.

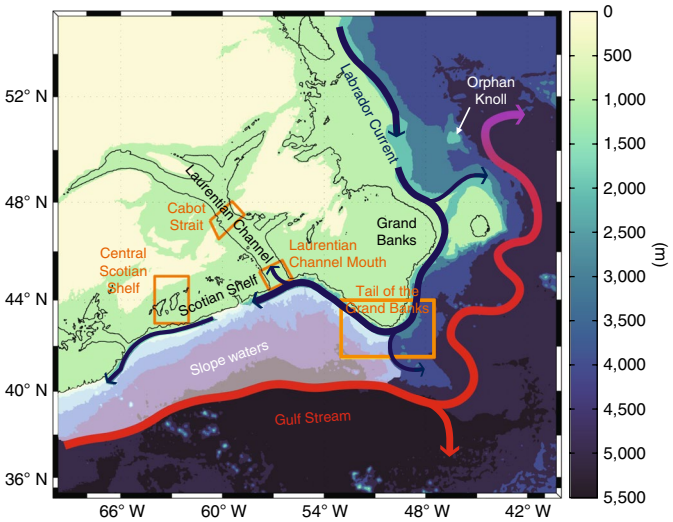

Fig. 1 | Schematic of the large-scale circulation in the northwest Atlantic. Labrador Current waters flow equatorwards along the shelf break. At the Grand Banks, the Labrador Current must take a sharp right-hand (westward) turn to flow along the shelf break and maintain a direct advective connection with the slope waters region (white shading) at the offshore edge of the Scotian Shelf and Laurentian Channel. Circulation on the slope mixes well-oxygenated Labrador Slope Water with oxygen-poor subtropical waters[31]. In turn, slope water masses and circulation influence water properties on the continental shelf[28]. Bathymetry is indicated by the colour scale and the 200 m isobath by the solid contour. Circulation schematics follow geostrophic currents[32].

Figure 2 shows updated historical time series for three well-studied sites on the Scotian Shelf and in the Gulf of Saint Lawrence that confirms the continued trajectories of previously reported trends[6,7,16]. Although the observations show large decadal-scale variability, the long-term average rate of O_2 decline at Cabot

[1]Joint Institute for the Study of the Atmosphere and the Ocean, Seattle, WA, USA. [2]University of Washington, Seattle, WA, USA. [3]Department of Earth and Planetary Sciences, McGill University, Montréal, Quebec, Canada. [4]Institució Catalana de Recerca i Estudis Avançats (ICREA), Barcelona, Spain. [5]Institut de Ciència i Tecnologia Ambientals, Universitat Autònoma de Barcelona, Cerdanyola del Vallès, Spain. [6]Graduate School of Oceanography, University of Rhode Island, Narragansett, RI, USA. [7]Department of Atmospheric and Oceanic Sciences, University of California, Los Angeles, CA, USA. [8]Department of Oceanography, Dalhousie University, Halifax, Nova Scotia, Canada. [9]Maurice Lamontagne Institute, Fisheries and Oceans Canada, Mont-Joli, Quebec, Canada. [10]NOAA Geophysical Fluid Dynamics Laboratory, Princeton, NJ, USA. *e-mail: mclaret@uw.edu

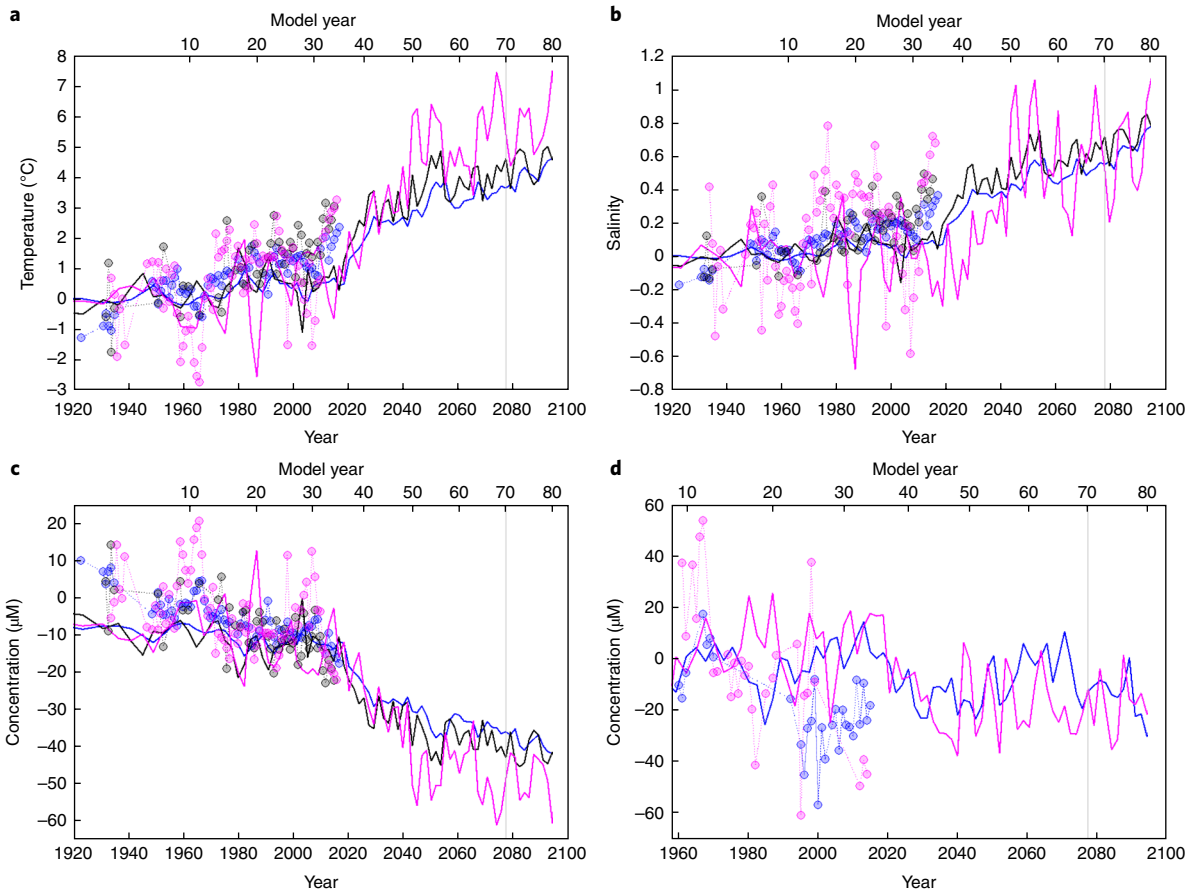

Fig. 2 | Warming, salinity increase and deoxygenation in the coastal northwest Atlantic. a–d, Observational anomaly time series (filled circles) show the change in potential temperature referenced to the surface (θ) (**a**), salinity (S) (**b**), O_2^{sat} (**c**) and O_2 (**d**) on the isopycnal $\sigma_\theta = 27.25\,kg\,m^{-3}$ at Cabot Strait (blue), the Laurentian Channel Mouth (black) and at 150 m in the central Scotian Shelf (magenta). Anomalies are relative to a time average computed between 1920 and 1960 for θ, S and O_2^{sat}. For O_2, the time average is between 1960 and 1970 at Cabot Strait and between 1961 and 1999 at the central Scotian Shelf. Standard error bars are given in Supplementary Figs. 1 and 2. The time series of change at the corresponding model locations (solid lines) are shown on a transformed time axis (upper axis) that roughly corresponds to the historical CO_2 trajectory (Methods). The vertical grey lines in each panel denote the year at which the modelled atmospheric p_{CO_2} doubles relative to the preindustrial value. Observed and modelled trends for each property at each location are provided in Supplementary Figs. 1 and 2. The depth evolution of isopycnal $\sigma_\theta = 27.25\,kg\,m^{-3}$ at Cabot Strait and the Laurentian Channel Mouth is shown in Supplementary Fig. 8.

Strait was $-0.51 \pm 0.24\,\mu M\,yr^{-1}$ between 1960 and 2015 on isopycnal $\sigma_\theta = 27.25\,kg\,m^{-3}$, whereas on the Central Scotian Shelf it was $-1.19 \pm 0.45\,\mu M\,yr^{-1}$ between 1961 and 2014 at a 150 m depth, more than twice as fast (Supplementary Fig. 1). The O_2 trend at Cabot Strait is indistinguishable from the trend of $-0.5\,\mu M\,yr^{-1}$ between 1958 and 2015 recently estimated from World Ocean Atlas data in waters of 100–400 m depth in the open ocean, south of the Scotian Shelf[3]. Oxygen concentrations can be conceptualized as the difference between an oxygen saturation concentration (O_2^{sat}) equal to the oxygen concentration the waters would have in equilibrium with the atmosphere given their temperature and salinity, and the Apparent Oxygen Utilization (AOU) due to the consumption of oxygen by heterotrophic organisms, such that $O_2 = O_2^{sat} - AOU$. The trends of O_2^{sat} are similar at the three sites (Fig. 2c (filled circles) and Supplementary Fig. 1), which reflects comparable trends of temperature and salinity (Fig. 2a,b (filled circles) and Supplementary Fig. 2). This similarity implies that the main difference behind the large change on the Scotian Shelf, relative to the Cabot Strait, is due to differences in the AOU.

To characterize the dynamics behind this dramatic historical deoxygenation, we analysed a high-resolution global coupled climate model forced by an idealized CO_2-driven global warming scenario (Methods). This model faithfully captures critical aspects of the northwest Atlantic circulation, specifically reducing a warm bias on the Scotian Shelf that is common to coarse-resolution models in which the Gulf Stream extends too far north[23]. Moreover, it simulates a spatial pattern of surface cooling in the subpolar North Atlantic and warming on the Scotian Shelf that agrees well with historical observations; in the simulation, this pattern of sea surface temperature change is linked to a slowing of the AMOC[10].

The model reproduces the general O_2^{sat} decline associated with increasing temperature and salinity at the three sites (solid lines in Fig. 2a–c). Thus, the model reveals a potential mechanism for the rapid deoxygenation observed on the Scotian Shelf: a change in the large-scale ocean circulation that shifts the balance of water masses in the region. However, the model does not reproduce the long-term decline of oxygen concentrations at the two sites at which measurements are available. The constant total oxygen concentration simulated at these sites by the model reflects a compensation of the O_2^{sat} decline by a similar decrease in AOU. Thus, it appears that the model captures the broad hydrographic change and O_2^{sat} decrease well, while it simulates a process that slows oxygen utilization (and thereby reduces AOU) that was not operating in nature during the historical period.

The northwest Atlantic shelf is thought to be particularly sensitive to climate variability due to its position near the crossroads of the subtropical and subpolar circulation at the nearby the Grand Banks of Newfoundland (Fig. 1), an underwater plateau that forces the Labrador Current to take a sharp right-hand (westward) turn to continue its trajectory as a western boundary current in contact with the shelf break. An association was previously found between the water column properties at the Tail of the Grand Banks (TGB) (that is, its southeastern tip (Fig. 1)), the position of the Gulf Stream and the strength of the AMOC in observations and models[10,23,25,26]: warmer temperatures at the TGB correspond to a more northward Gulf Stream trajectory and a weaker AMOC. Moreover, decadal variability in the Labrador Current transport around the TGB to the Scotian Shelf[27], including to the Laurentian Channel Mouth[28], was found to influence the properties of slope waters (that is, water masses at depths greater than 200 m and less than 3,000 m, shaded white in Fig. 1). As half of the O_2 decline on the northwest Atlantic shelf was shown to be due to a rising proportion of oxygen-poor subtropical waters[7], we hypothesized that the rapid twentieth century O_2 decline was due to a retreat of the Labrador Current and the increasing presence of Gulf Stream waters at the TGB.

To test for this dynamical change, we calculated the historical depths of two subsurface isopycnals at the TGB from high-quality observations in the Hydrobase data repository (Methods). Both isopycnals shoal by more than 700 m from the core of the Labrador Current to the subtropical side of the Gulf Stream (Supplementary Fig. 3); thus, a reduced presence of the Labrador Current at the TGB would be expected to result in a deepening of these isopycnals over time. Indeed, the data show the isopycnal that enters the Laurentian Channel ($\sigma_\theta = 27.25\,kg\,m^{-3}$) deepened at the TGB by $0.48 \pm 0.2\,m\,yr^{-1}$ between 1920 and 2010 (filled circles in Fig. 3a), and an even faster deepening trend occurred on the denser isopycnal ($\sigma_1 = 32.2\,kg\,m^{-3}$) with a rate of $1.30 \pm 0.36\,m\,yr^{-1}$ over the same time period (filled circles in Fig. 3b). The simulated isopycnals in the same region also deepen as the model responds to the warming effect of an atmospheric CO_2 increase (solid lines in Fig. 3).

The deepening of isopycnals reflects a buoyancy gain by the upper water column, due to an increase in buoyant subtropical waters relative to dense subpolar waters, consistent with the modelled change in horizontal circulation (Supplementary Fig. 4). Under doubled CO_2, the simulated Labrador Current weakens by as much as 8–10 Sv ($1\,Sv \equiv 10^6\,m^3\,s^{-1}$ (definition in Methods)) north of the Grand Banks, as it approaches Orphan Knoll (Supplementary Fig. 4). Associated with this reduced transport, the boundary between the cyclonic subpolar circulation and anticyclonic Gulf Stream migrates north, which increases the probability that the Gulf Stream and/or its associated eddies impinge on the TGB. The shift in the Gulf Stream position and the Labrador Current slowdown is associated with a weakening of the AMOC[10,23], both of which may also be related to a weakening of the wind stress curl on the subpolar gyre simulated by the climate model (Supplementary Fig. 5). An important association between the large-scale wind field and the northward excursions of the Gulf Stream is supported by recent findings that show that the variability in northwest Atlantic shelf waters correlates with the interannual variability in the wind stress, with the mean position of the Gulf Stream being closely tied to the mean zero wind stress curl line[28]. The consistency between the observations and the simulation strongly suggests that a climate-driven dynamical shift, towards enhanced impingement of the Gulf Stream on the TGB, is at least partly responsible for the shrinking influence of the Labrador Current waters and the associated deoxygenation of the Scotian Shelf and Gulf of St Lawrence.

Given that the simulated retreat of the Labrador Current and decrease of O_2^{sat} under warming appear to be consistent with the observed historical changes, we provide further analysis of the impacts on oxygen concentrations under continued warming as an indication of potential future trends (red lines in Supplementary Figs. 1 and 2). Focusing on an isopycnal surface, as the modelled Labrador Current continues to retreat, the supply of well-oxygenated waters rounding the TGB dwindles (Supplementary Video) and a large decrease of oxygen occurs throughout the coastal region, but with significant spatial variation (Fig. 4). The modelled O_2^{sat} concentrations decrease throughout the coastal region as the waters of a given density become warmer and saltier. This decrease is most pronounced where the isopycnal impinges on the continental shelf and within the Laurentian Channel (Fig. 4b). The coastal O_2^{sat} decrease is amplified by increases of AOU to cause large O_2 decreases along the path of the Labrador Current and around the margin of the Grand Banks. However, it is opposed by AOU decreases (Fig. 4c) in the more southern coastal regions and Laurentian Channel, which mitigates the simulated O_2 decrease (Fig. 4a).

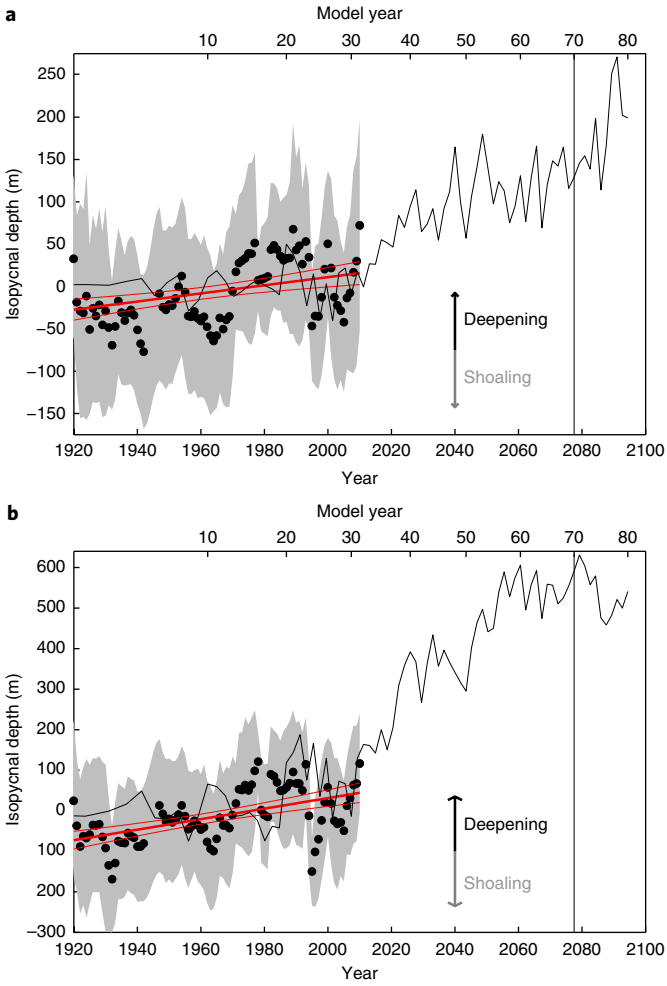

Fig. 3 | Two isopycnal depth anomalies at the Tail of the Grand Banks. **a**,**b**, Depth anomalies are shown for $\sigma_\theta = 27.25\,kg\,m^{-3}$ (**a**) and $\sigma_1 = 32.2\,kg\,m^{-3}$ (**b**). Observations (filled circles) are three-year averages from the region shown in Fig. 1, calculated using springtime (April, May and June) data only, and are plotted with their s.d. (shaded area). Also shown is a linear regression (thick red line) for each, with the associated 95% confidence intervals (thin red lines). Model-simulated isopycnal depth anomalies, averaged over the same region for the warming simulation using the transformed time axis (Fig. 2 caption) are shown as solid black lines. A positive change in isopycnal depth corresponds to isopycnal deepening, interpreted as a gain of buoyant subtropical waters above the given isopycnal. See Methods for details.

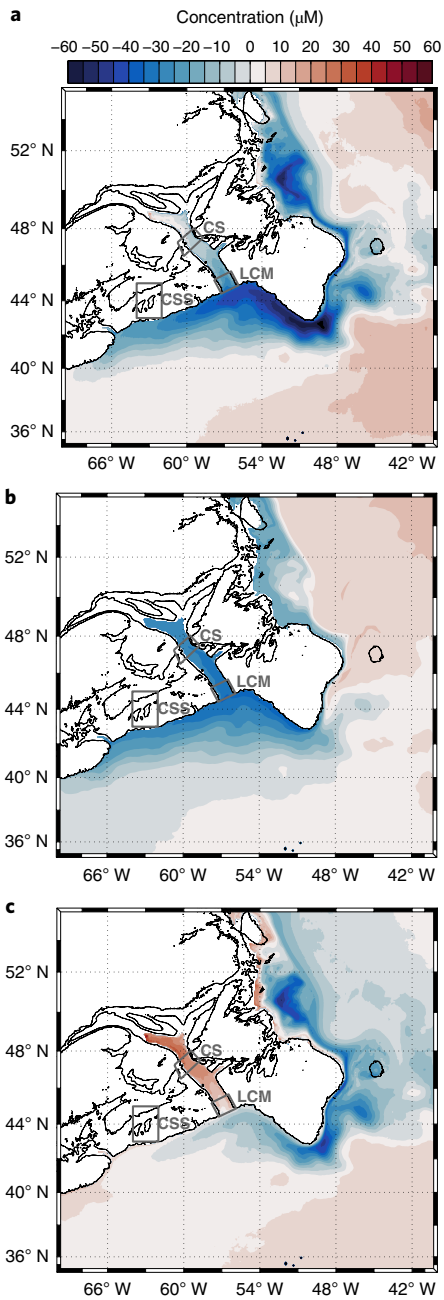

Fig. 4 | Decomposition of the modelled oxygen decline with warming in the northwestern Atlantic. a–c, Isopycnal maps on $\sigma_\theta = 27.25\,kg\,m^{-3}$ of the oxygen (O_2) change (**a**) and its decomposition into changes of O_2^{sat} (**b**) and AOU (**c**). The differences are computed relative to the control preindustrial experiment and averaged over the last 20 model years. The locations for the time series shown in Fig. 2 are enclosed within grey polygons. LCM, Laurentian Channel Mouth; CS, Cabot Strait; CSS, central Scotian Shelf.

Further mechanistic understanding of the simulated O_2^{sat} and AOU changes are provided by a water-mass mixing model on an isopycnal surface (Supplementary Information). This approach shows that the deoxygenation is primarily driven by a shift in ocean circulation, with additional contributions from warming and reduced ventilation of the Labrador Current endmember. Taking the Laurentian Channel Mouth as a representative site, we found that the Labrador Current retreat drives about two-thirds of the simulated oxygen loss (Supplementary Tables 1–3). The remaining changes are caused by changes in the Labrador Current endmember properties that result from a decrease in O_2^{sat} due to warming, and an increase in the endmember AOU as the intensified near-surface stratification impedes the formation of newly ventilated waters (Supplementary Fig. 6). A long-term trend towards a reduced ventilation and the retreat of Labrador Current waters is consistent with palaeoceanographic reconstructions that show a slowdown of the AMOC and reduced ventilation in the Labrador Sea, where the Labrador Current is formed, over the past 150 years[21]. As a result of these dynamical changes, the O_2^{sat} change at the time of CO_2 doubling is as much as $-32.8\,\mu M$ in the northwest Atlantic slope and the Laurentian Channel (Fig. 4b and Supplementary Table 2), whereas the average O_2^{sat} decline in the upper North Atlantic (above 300 m depth) in the warming simulation is only $-6.3\,\mu M$. In contrast, the simulated AOU decrease is in direct disagreement with historical records (Fig. 2 and Supplementary Fig. 1). This disagreement reflects a decrease in respiration rates along the pathway of the circulation between the endmembers (Supplementary Table 2), due to a reduction of simulated nutrient supply to the surface. The model inaccuracy probably arises from the relative simplicity of the biogeochemical model, which lacks many features, such as anthropogenic nutrient inputs and interactions with the benthos. We therefore expect that future O_2 declines in this region may be significantly larger than simulated by the model, and could feasibly exceed the reduction in saturation.

The deoxygenation observed in the northwest Atlantic shelf is already altering the regional ecosystem[16,29] and, as shown by our results, is likely to become much more pronounced with continued global warming. These results emphasize the importance that open ocean dynamics can play in regional oxygen changes[5], and explain the quasi-centennial O_2^{sat} trends of about $-0.21 \pm 0.03\,\mu M\,yr^{-1}$ observed between 1923 and 2017 in the Gulf of St Lawrence (Supplementary Fig. 1). This change in saturation concentration alone is more than double the total oxygen trend reported over the past 50 years in the upper layers of the North Atlantic, being $-0.075\,\mu M\,yr^{-1}$ averaged above 1,200 m (ref. [2]) and about $-0.099\,\mu M\,yr^{-1}$ for the upper and intermediate waters[15]. Yet, given the pronounced decadal variability (Fig. 2), even the strong local trends in the Scotian Shelf would be undetectable without long observational time series. Moreover, because local circulation dynamics are difficult to resolve in global models, they may harbour surprises in other coastal regions. Finally, we speculate that the decline of oxygen concentrations on the northwest Atlantic shelf is a sensitive indicator of large-scale dynamical shifts offshore, which are potentially linked with a centennial-scale slowdown of the AMOC[10] and may ultimately influence the oxygen variability of the open North Atlantic[30].

Methods

Methods, including statements of data availability and any associated accession codes and references, are available at https://doi.org/10.1038/s41558-018-0263-1.

Received: 15 January 2018; Accepted: 27 July 2018;
Published online: 17 September 2018

References

1. Helm, K. P., Bindoff, N. L., & Church, J. A. Observed decreases in oxygen content of the global ocean.*Geophys. Res. Lett.* **38**, L23602 (2011).
2. Schmidtko, S., Stramma, L. & Visbeck, M. Decline in global oceanic oxygen content during the past five decades. *Nature* **542**, 335–339 (2017).
3. Ito, T., Minobe, S., Long, M. C. & Deutsch, C. Upper ocean O_2 trends: 1958–2015. *Geophys. Res. Lett.* **44**, 4214–4223 (2017).
4. Breitburg, D. et al. Declining oxygen in the global ocean and coastal waters.*Science* **359**, eaam7240 (2018).
5. Levin, L. A. Manifestation, drivers, and emergence of open ocean deoxygenation. *Ann. Rev. Mar. Sci.* **10**, 229–260 (2018).

6. Petrie, B. & Yeats, P. Annual and interannual variability of nutrients and their estimated fluxes in the Scotian Shelf—Gulf of Maine region. *Can. J. Fish. Aquat. Sci.* **57**, 2536–2546 (2000).
7. Gilbert, D., Sundby, B., Gobeil, C., Mucci, A. & Tremblay, G.-H. A seventy-two-year record of diminishing deep-water oxygen in the St. Lawrence estuary: the northwest Atlantic connection. *Limnol. Oceanogr.* **50**, 1654–1666 (2005).
8. Gilbert, D., Rabalais, N. N., Díaz, R. J. & Zhang, J. Evidence for greater oxygen decline rates in the coastal ocean than in the open ocean. *Biogeosciences* **7**, 2283–2296 (2010).
9. Dufour, C. O. et al. Role of mesoscale eddies in cross-frontal transport of heat and biogeochemical tracers in the Southern Ocean. *J. Phys. Oceanogr.* **45**, 3057–3081 (2015).
10. Caesar, L., Rahmstorf, S., Robinson, A., Feulner, G. & Saba, V. Observed fingerprint of a weakening Atlantic Ocean overturning circulation. *Nature* **556**, 191–196 (2018).
11. Keeling, R. F., Körtzinger, A. & Gruber, N. Ocean deoxygenation in a warming world. *Ann. Rev. Mar. Sci.* **2**, 199–229 (2010).
12. Long, M. C., Deutsch, C. & Ito, T. Finding forced trends in oceanic oxygen. *Glob. Biogeochem. Cycles* **30**, 381–397 (2016).
13. Johnson, G. C. & Gruber, N. Decadal water mass variations along 20° W in the Northeastern Atlantic Ocean. *Prog. Oceanogr.* **73**, 277–295 (2007).
14. Frölicher, T. L., Joos, F., Plattner, G.-K., Steinacher, M. & Doney, S. C. Natural variability and anthropogenic trends in oceanic oxygen in a coupled carbon cycle-climate model ensemble. *Glob. Biogeochem. Cycles* **23**, GB1003 (2009).
15. Stendardo, I. & Gruber, N. Oxygen trends over five decades in the North Atlantic.*J. Geophys. Res. Oceans* **117**, C11004 (2012).
16. Brennan, C. E., Blanchard, H. & Fennel, K. Putting temperature and oxygen thresholds of marine animals in context of environmental change: a regional perspective for the Scotian Shelf and Gulf of St. Lawrence. *PLoS ONE* **11**, 1–27 (2016).
17. Thibodeau, B., de Vernal, A., Hillaire-Marcel, C. & Mucci, A. Twentieth century warming in deep waters of the Gulf of St. Lawrence: A unique feature of the last millennium. *Geophys. Res. Lett.* **37**, L17604 (2010).
18. Genovesi, L. et al. Recent changes in bottom water oxygenation and temperature in the Gulf of St. Lawrence: micropaleontological and geochemical evidence. *Limnol. Oceanogr.* **56**, 1319–1329 (2011).
19. Keigwin, L., Sachs, J. & Rosenthal, Y. A 1600-year history of the Labrador Current off Nova Scotia. *Clim. Dynam.* **12**, 53–62 (2003).
20. Sherwood, O. A., Lehmann, M. F., Schubert, C. J., Scott, D. B. & McCarthy, M. D. Nutrient regime shift in the western North Atlantic indicated by compound-specific δ15N of deep-sea gorgonian corals. *Proc. Natl Acad. Sci. USA* **108**, 1011–1015 (2011).
21. Thornalley, D. J. R. et al. Anomalously weak Labrador Sea convection and Atlantic overturning during the past 150 years. *Nature* **556**, 227–230 (2018).
22. Loder, J. W., van der Baaren, A. & Yashayaev, I. Climate comparisons and change projections for the Northwest Atlantic from six CMIP5 models. *Atmos. Ocean* **53**, 529–555 (2015).
23. Saba, V. S. et al. Enhanced warming of the Northwest Atlantic Ocean under climate change. *J. Geophys. Res. Oceans* **121**, 118–132 (2016).
24. Lavoie, D., Lambert, N. & Gilbert, D. Projections of future trends in biogeochemical conditions in the northwest Atlantic using CMIP5 Earth system models. *Atmos. Ocean* https://doi.org/10.1080/07055900.2017.1401973 (2017).
25. Joyce, T. M. & Zhang, R. On the path of the Gulf Stream and the Atlantic Meridional Overturning Circulation. *J. Clim.* **23**, 3146–3154 (2010).
26. Buckley, M. W. & Marshall, J. Observations, inferences, and mechanisms of the Atlantic Meridional Overturning Circulation: a review. *Rev. Geophys.* **54**, 5–63 (2016).
27. Petrie, B. & Drinkwater, K. Temperature and salinity variability on the Scotian Shelf and in the Gulf of Maine 1945–1990. *J. Geophys. Res. Oceans* **98**, 20079–20089 (1993).
28. Peterson, I., Greenan, B., Gilbert, D. & Hebert, D. Variability and wind forcing of ocean temperature and thermal fronts in the Slope Water region of the Northwest Atlantic. *J. Geophys. Res. Oceans* **122**, 7325–7343 (2017).
29. Bianucci, L., Fennel, K., Chabot, D., Shackell, N. & Lavoie, D. Ocean biogeochemical models as management tools: a case study for Atlantic wolffish and declining oxygen. *ICES J. Mar. Sci.* **73**, 263–274 (2016).
30. Tagklis, F., Bracco, A. & Ito, T. Physically driven patchy O_2 changes in the North Atlantic Ocean simulated by the CMIP5 Earth system models. *Glob. Biogeochem. Cycles* **31**, 1218–1235 (2017).
31. Gatien, M. G. A study in the slope water region south of Halifax. *J. Fish Res. Board Can.* **33**, 2213–2217 (1976).
32. Bisagni, J. J., Gangopadhyay, A. & Sanchez-Franks, A. Secular change and inter-annual variability of the Gulf Stream position, 1993–2013, 70°–55° W. *Deep Sea Res. I* **125**, 1–10 (2017).

Acknowledgements

The authors thank A. Cogswell and R. Pettipas from Fisheries and Oceans Canada for providing hydrographic data in the central Scotian Shelf and C. E. Brennan for providing the data for the oxygen time series in the central Scotian Shelf. The authors also acknowledge many scientists at NOAA GFDL that configured and ran the climate model, without whose efforts this work would not have been possible. This project has received funding from the European Research Council under the European Union's Horizon 2020 research and innovation programme (grant no. 682602). E.D.G. acknowledges financial support from the Spanish Ministry of Economy and Competitiveness through the Mara de Maeztu Programme for Centres/Units of Excellence (MDM-2015-0552). The Canadian Foundation for Innovation provided the computing resources for model analysis. D.B. acknowledges support from NOAA grant NA15NOS4780186.

Author contributions

E.D.G., J.B.P. and D.B. conceived the study. M.C., D.G. and K.F. assembled and analysed the observational data. M.C. and D.B. performed the model output analyses. J.P.D. and E.D.G. participated in the design of the CM2.6-miniBLING experiments. M.C., E.D.G., J.B.P. and D.B. wrote the first draft of the manuscript. All the authors discussed the results and provided input to the manuscript.

Competing interests

The authors declare no competing Interests.

Additional information

Supplementary information is available for this paper at https://doi.org/10.1038/s41558-018-0263-1.

Reprints and permissions information is available at www.nature.com/reprints.

Correspondence and requests for materials should be addressed to M.C.

Publisher's note: Springer Nature remains neutral with regard to jurisdictional claims in published maps and institutional affiliations.

Methods

Observational data, instrument accuracy and analyses. Hydrographic data for Cabot Strait and the Laurentian Channel Mouth are compiled, maintained and quality controlled by Fisheries and Oceans Canada. Temperature data were sampled before 1943 using reversing thermometers mounted on bottles (accuracy ±0.01 °C), after 1943 using mechanical bathythermographs (accuracy ±0.1 °C) and from 1969 onwards a variety of conductivity–temperature–depth (CTD) models were used with accuracy of ±0.01 °C or better[7]. Salinity data before 1969 were sampled from bottles (accuracy ±0.05) and after 1969 using CTDs (accuracy of ±0.01 or better)[7]. Oxygen data are collected, maintained and quality controlled by Fisheries Ocean Canada. These oxygen data were measured using Winkler titrations with an accuracy of ±0.3–5 μM (ref. [7]). Time series are constructed by spatially averaging data interpolated on isopycnal $\sigma_\theta = 27.25\,\mathrm{kg\,m^{-3}}$ over areas delimited by four coordinate pairs (Fig. 1). For Cabot Strait these are (60.74° W, 47.26° N), (59.43° W, 48.03° N), (58.70° W, 47.50° N) and (60.22° W, 46.52° N), and for the Laurentian Channel Mouth they are (57.83° W, 45.20° N), (57.24° W, 44.42° N), (55.86° W, 44.88° N) and (56.46° W, 45.67° N).

At the central Scotian Shelf, hydrographic data are quality controlled by Fisheries Ocean Canada. Before late 1960s, temperature and salinity data were sampled using bottles with typical accuracies of ±0.01 °C and ±0.01–0.03‰ (ref. [33]), respectively. In the mid-to-late 1960s, hydrographic measurements were made with an early CTD that had an accuracy of ±0.01 °C for temperature and ±0.01 for salinity, which improved to ±0.001 °C for temperature and ±0.003 for salinity with the introduction of modern CTDs in the late 1980s (B. Petrie, personal communication). Oxygen data were compiled and quality controlled by C. E. Brennan. Oxygen data between 1961 and 1999 were measured using Winkler titration (the standard accuracy for this method performed on ships using bottle samples is ±0.9–1.8 μM (ref. [33])) and between January 2012 and December 2014 were measured using Aanderaa optodes mounted on benthic pods (accuracy of ±8 μM with a two-point calibration (C. E. Brennan, personal communication)). The hydrographic time series correspond to data averaged over a box that extends zonally from 62° W to 64° W, meridionally from 43° N to 45° N and vertically from 145 to 155 m. The oxygen time series between 1961 and 1999 at a 150 m depth is based on reported oxygen anomaly time series[6] plus a mean value of 179.7 μM computed from a subset of the original data set[16] as the complete data set is unavailable. For the period from January 2012 to December 2014, oxygen data in this region are interpolated at 150 m from high-resolution observations of two benthic pods[16], one at a depth of 133 m (63.10° W, 44.09° N) and the other one at 160 m (63.19° W, 43.91° N).

Historical time series of the depth of two isopycnals at the TGB are computed using data extracted from HydroBase3, which is a global database of observed profiles that is quality controlled, compiled and made available by the Woods Hole Oceanographic Institution (WHOI). The data were extracted for the time period between 1920 and 2012, and the region that extends zonally from 53° W to 47.5° W and meridionally from 41.5° N to 44° N (Fig. 1). Only data flagged as 'good measurement' are considered. The resulting subdata comprise vertical profiles from bottles (86%), CTD casts (9%) and Argo floats (5%). Historical hydrographic data were sampled using bottles until the 1980s, with an accuracy of ±0.01–0.02 °C for temperature and ±0.01–0.03‰ for salinity as reported for measurements carried at WHOI[33]. CTDs mounted on rosettes were introduced in the late 1960s and have typical temperature and salinity accuracies of ±0.001 °C and ±0.003, respectively. Finally, the Argo float program started in the early 2000s and CTD mounted on these floats are less accurate (±0.002 °C for temperature and ±0.01 for salinity) than those used on ships, as they are not routinely calibrated (http://www.argo.ucsd.edu/Data_FAQ.html#accurate). Observational analyses at the TGB are limited to springtime observations because the spring months (April, May and June) are the best sampled, with 61% of all the data, and because observations are sparse in other months, particularly before 1950. By limiting our analysis to a single well-sampled season, we avoid aliasing seasonal variability in our multidecadal time series. First, time series of isopycnal depths were obtained by cubic interpolation of a specific density using hydrographic vertical profiles. Second, we constructed a spatially varying springtime isopycnal depth by averaging over all the observations in 0.5° × 0.5° subdomains of the TGB region. Third, we calculated isopycnal depth anomalies by subtracting the appropriate climatological mean from every observation within these subdomains. These anomalies were then averaged in overlapping three-year windows to arrive at the black dots in Fig. 3a,b. This procedure for calculating anomalies helps minimize the possibility for mistakenly interpreting variability in the location in which the observations were collected in the larger box as a change in properties at the TGB. Finally, a linear least squares regression was performed to find the temporal trend over the time series of anomalies. The resulting observational time series are compared with the climate model output by computing isopycnal depth differences between warming and preindustrial control scenarios averaged over the TGB and over each model year.

For all the analyses, density is derived from the hydrographic data using the equation of state EOS-80 (ref. [34]) because it is available in the software (NOAA/PMEL Ferret) that is amenable to the analysis of large model output. Although EOS-80 has been superseded by the International Thermodynamic Equation Of Seawater-2010 (TEOS-10), the two algorithms return near identical density values in our region of interest. We quantified these differences in terms of isopycnal depth anomaly time series. The root mean square difference between time series using TEOS-10 and EOS-80 is 1.9 m for $\sigma_\theta = 27.25\,\mathrm{kg\,m^{-3}}$ and 2.8 m for $\sigma_1 = 32.3\,\mathrm{kg\,m^{-3}}$, that is, much smaller than the standard error (shaded areas in Fig. 3). Additionally, the differences in isopycnal deepening trends between 1920 and 2010 are about 0.01 m, which is also much smaller than 95% confidence intervals, which are ±0.2 m for $\sigma_\theta = 27.25\,\mathrm{kg\,m^{-3}}$ and ±0.35 m for $\sigma_1 = 32.3\,\mathrm{kg\,m^{-3}}$.

Climate model. The Geophysical Fluid Dynamics Laboratory (GFDL) climate model CM2.6 is a high-resolution coupled atmosphere–ocean–ice global model that includes a reduced-complexity ocean biogeochemical model[9]. The ocean component (MOM5) has a spatial resolution of 1/10° and 50 vertical levels, and the biogeochemical model (miniBLING[35]) consists of three prognostic tracers—dissolved inorganic carbon, phosphate and oxygen. Human-induced biogeochemical inputs, such as nutrient loading, are not implemented.

The fully coupled model was spun up for 72 years with atmospheric CO_2 fixed at a preindustrial concentration (286 ppm). After the spin-up phase, two different scenarios were integrated for an additional period of 80 years: a preindustrial control scenario in which atmospheric CO_2 is held constant, and a warming scenario in which CO_2 is increased at an annual rate of 1% until doubled. After doubling, which occurs at model year 70, atmospheric CO_2 was held constant for ten additional years. We analysed the full 80-year period of both simulations. Numerical time series for any given property χ are constructed as $\chi(t) = \chi(t=0) + \Delta\chi(t)$, where $\chi(t=0)$ is the value at the preindustrial initial time (year 1860), and $\Delta\chi$ is the difference between the warming case and the same model year of the preindustrial control case. In this way, the influence of any model drift is minimized.

Modelled (MOD) and observational (OBS) time dimensions are related through atmospheric CO_2. The climate model is forced by a rapid increase in CO_2 that resembles the RCP6 scenario, following $CO_2^{MOD}(t^*) = 286\ e^{0.01\,t^*}$, where $t^* \in [0,80]$ is the model time. Historical and projected future CO_2 time series are approximated by a quadratic polynomial of the form $CO_2^{OBS}(t) = 0.01005\,(t-1860)^2 - 0.9605\,(t-1860) + 309.3$ for $t > 1860$, being $CO_2^{OBS} = 286$ at $t = 1860$. The modelled time dimension is therefore transformed by a factor r that fulfils $CO_2^{MOD}(t^*) = CO_2^{OBS}(rt^*)$ (Supplementary Fig. 7). Our intention was to put the modelled time series on a time axis that roughly corresponds to the historical CO_2 trajectory. We acknowledge that transforming the time axis to relate the idealized model, following a convention of 1% per year increase in atmospheric CO_2, to the historical period, when atmospheric CO_2 was increasing at a slower rate, does not account for other forced changes due to atmospheric aerosols, non-CO_2 GHGs and ozone.

Most of the model analyses were performed on isopycnal surfaces, rather than at fixed depths, to avoid conflating shifts in water-mass characteristics with the heaving of isopycnals. We focused on $\sigma_\theta = 27.25\,\mathrm{kg\,m^{-3}}$ because its simulated depth is close to the observed depth range within the Laurentian Channel (Supplementary Fig. 8) and it remains isolated from the surface throughout the region, which thus avoids any influence from local air–sea exchange. For the Scotian Shelf, the analyses were performed on the 150 m horizontal level, where most measurements are available.

Quasi-streamfunction and wind stress curl. The quasi-streamfunction Ψ is defined so that $F_X \equiv -\partial\Psi/\partial y$ and $F_Y \equiv \partial\Psi/\partial x$, where the zonal flow is $F_X = \int_{z_1}^{z_0} u\,\mathrm{d}z$ and the meridional is $F_Y = \int_{z_1}^{z_0} v\,\mathrm{d}z$, u and v being the horizontal velocity components. These flows are depth integrated over the upper 1,000 m because our interest lies in the upper ocean circulation. Hence, the net vertical transport is non-zero or, in other words, the lateral flow is not fully divergence-free, and therefore we called it quasi-streamfunction. Flows are computed online in the model, saved every five days and solved for Ψ after cross-differentiation of the F_X and F_Y definitions. Finally, we averaged Ψ over the last 20 model years. This definition of Ψ has units of volume Sverdrup ($1\ \mathrm{Sv} \equiv 10^6\,\mathrm{m^3\,s^{-1}}$).

The curl of the wind stress vector $\boldsymbol{\tau} = (\tau_x, \tau_y)$ is approximated using finite differences as $\nabla_h \times \boldsymbol{\tau} \simeq \Delta\tau_y/\Delta x - \Delta\tau_x/\Delta y$. To unveil the large-scale pattern over the North Atlantic we take $\Delta x = \Delta y = 2°$ because grid spacings smaller than this threshold obscure the basin-scale distribution.

Data availability. The hydrographic data at Cabot Strait, the Laurentian Channel Mouth and the central Scotian Shelf come from the CLIMATE database (http://www.bio-iob.gc.ca/science/data-donnees/base/data-donnees/climate-climat-en.php). Oxygen data at Cabot Strait and for the central Scotian Shelf are available from the BioChem database (http://www.dfo-mpo.gc.ca/science/data-donnees/biochem/index-eng.html). Historical data at the TGB has been extracted from the public global database HydroBase3 website (http://www.whoi.edu/science/PO/hydrobase/php/index.php). The CM2.6-miniBLING model output is available upon request from J.P.D (john.dunne@noaa.gov). Bathymetric data comes from the 2-minute Gridded

Global Relief Data (ETOPO2) v2, which is publicly available (https://www.ngdc.noaa.gov/mgg/global/etopo2.html).

References

33. Warren, B. A. Nansen-bottle stations at the Woods Hole Oceanographic Institution. *Deep Sea Res. I* **55**, 379–395 (2008).
34. Millero, F. J., Chen, C.-T., Bradshaw, A. & Schleicher, K. A new high pressure equation of state for seawater. *Deep Sea Res. A* **27**, 255–264 (1980).
35. Galbraith, E. D. et al. Complex functionality with minimal computation: promise and pitfalls of reduced-tracer ocean biogeochemistry models. *J. Adv. Model. Earth Syst.* **7**, 2012–2028 (2015).

nature climate change

SUPPLEMENTARY INFORMATION

https://doi.org/10.1038/s41558-018-0263-1

In the format provided by the authors and unedited.

Rapid coastal deoxygenation due to ocean circulation shift in the northwest Atlantic

Mariona Claret[1,2,3]*, Eric D. Galbraith[3,4,5], Jaime B. Palter[6], Daniele Bianchi[7], Katja Fennel[8], Denis Gilbert[9] and John P. Dunne[10]

[1]Joint Institute for the Study of the Atmosphere and the Ocean, Seattle, WA, USA. [2]University of Washington, Seattle, WA, USA. [3]Department of Earth and Planetary Sciences, McGill University, Montréal, Quebec, Canada. [4]Institució Catalana de Recerca i Estudis Avançats (ICREA), Barcelona, Spain. [5]Institut de Ciència i Tecnologia Ambientals, Universitat Autònoma de Barcelona, Cerdanyola del Vallès, Spain. [6]Graduate School of Oceanography, University of Rhode Island, Narragansett, RI, USA. [7]Department of Atmospheric and Oceanic Sciences, University of California, Los Angeles, CA, USA. [8]Department of Oceanography, Dalhousie University, Halifax, Nova Scotia, Canada. [9]Maurice Lamontagne Institute, Fisheries and Oceans Canada, Mont-Joli, Quebec, Canada. [10]NOAA Geophysical Fluid Dynamics Laboratory, Princeton, NJ, USA. *e-mail: mclaret@uw.edu

SUPPLEMENTARY FIGURES

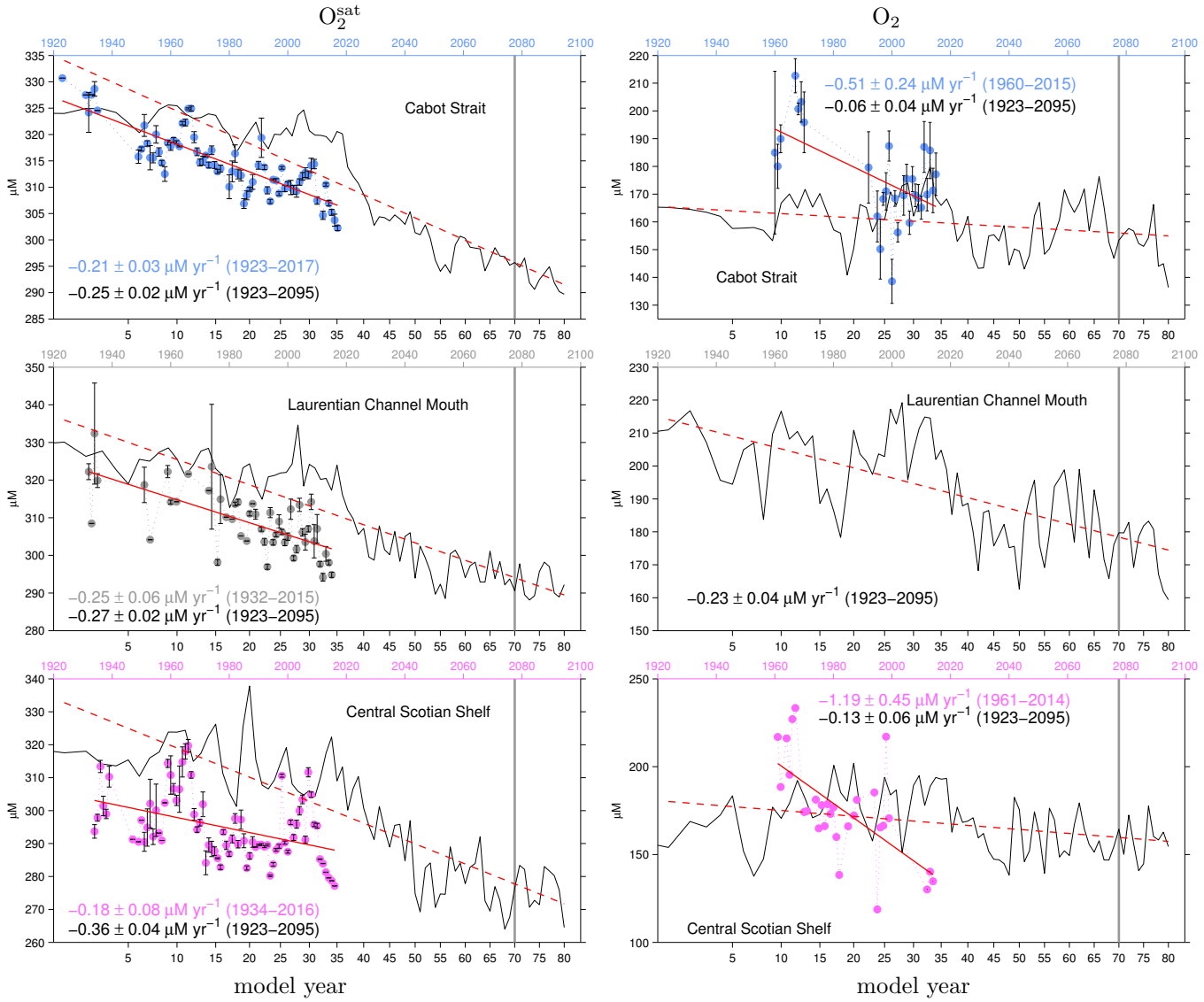

Figure S1. **Observational (dots) and modeled (solid black lines) deoxygenation time series in the Laurentian Channel and the Scotian Shelf.** Time series of oxygen saturation concentration (O_2^{sat}) and oxygen (O_2) on isopycnal $\sigma_\theta = 27.25\,\mathrm{kg\,m^{-3}}$ at Cabot Strait (blue) and at the Laurentian Channel Mouth (gray) and at 150 m depth in the central Scotian Shelf (magenta) plus/minus one standard error. For the O_2 time series at the central Scotian Shelf, only the standard deviation is known between 1961 and 1999 (24 μM, ref [6]), and between 2012 and 2014 the standard error is less than 0.2 μM given the high-frequency resolution of the benthic pod data. Observed and modeled trends are provided with 95% confidence intervals. These trends correspond to the red lines shown, solid lines for observations and dashed lines for model. Vertical solid line denotes the year at which modeled atmospheric pCO_2 is doubled relative to the pre-industrial 1860 historical value. See Methods for more data and analyses details.

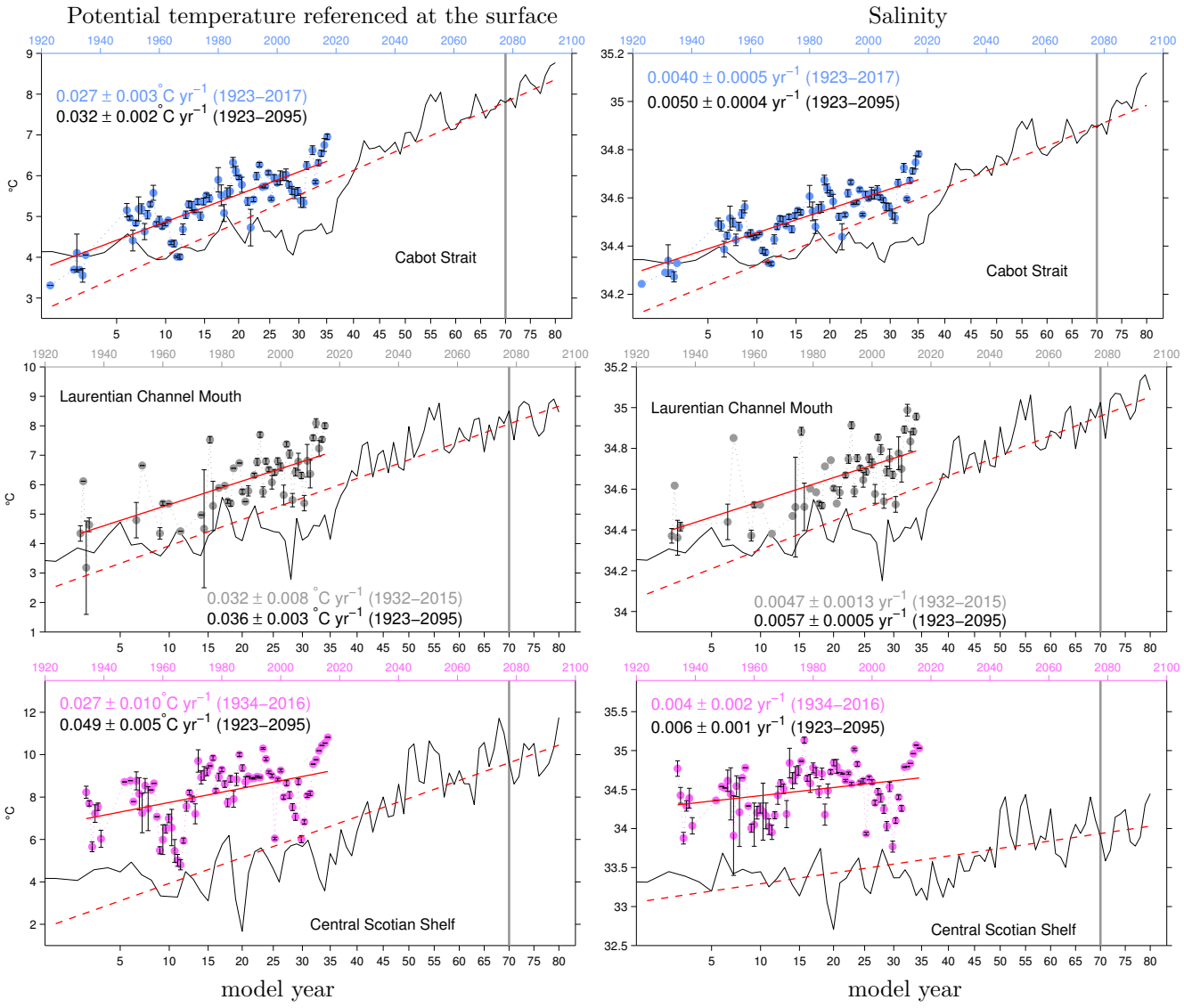

Figure S2. **Observational (dots) and modeled (solid black lines) hydrographic time series in the Laurentian Channel and the Scotian Shelf.** Same as Figure S1 for potential temperature and salinity.

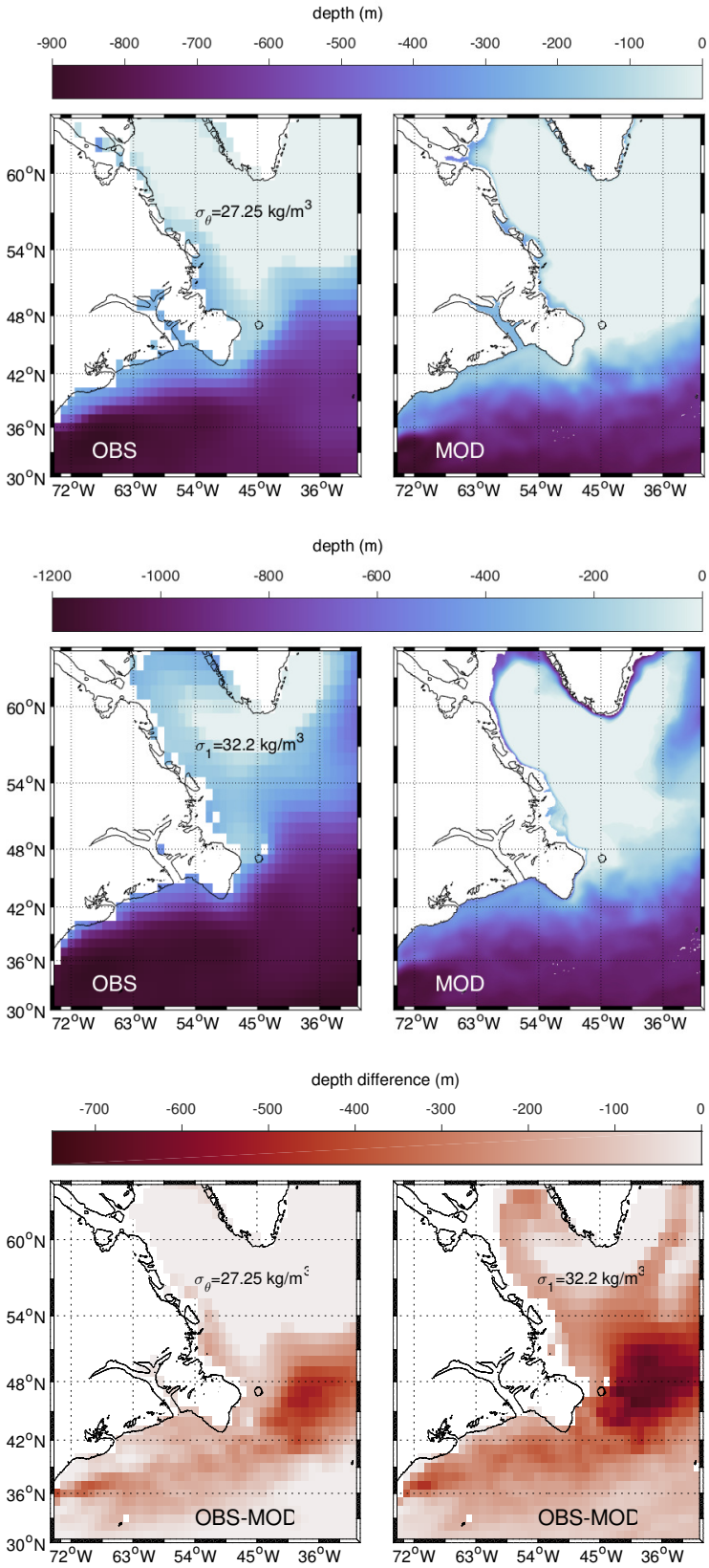

Figure S3. **Winter climatology for the northwest Atlantic of the depth of isopycnals $\sigma_\theta = 27.25\,\mathrm{kg\,m^{-3}}$ (top panels) and $\sigma_1 = 32.2\,\mathrm{kg\,m^{-3}}$ (middle panels) from observations (left) and model (right). Bottom panels show depth differences between observations and model for both isopycnals.** Observational data is from the World Ocean Atlas 2013 (https://www.nodc.noaa.gov/OC5/woa13/woa13data.html) and spans from 1955 to 2012, while modeled output is from the pre-industrial *control* scenario forced with atmospheric $p\mathrm{CO}_2$ 1860 historical value. The 200 m isobath is indicated for reference. Despite the notable differences between observations and model, in both cases isopycnals outcrop in the Labrador Sea and east of the Grand Banks for $\sigma_\theta = 27.25\,\mathrm{kg\,m^{-3}}$.

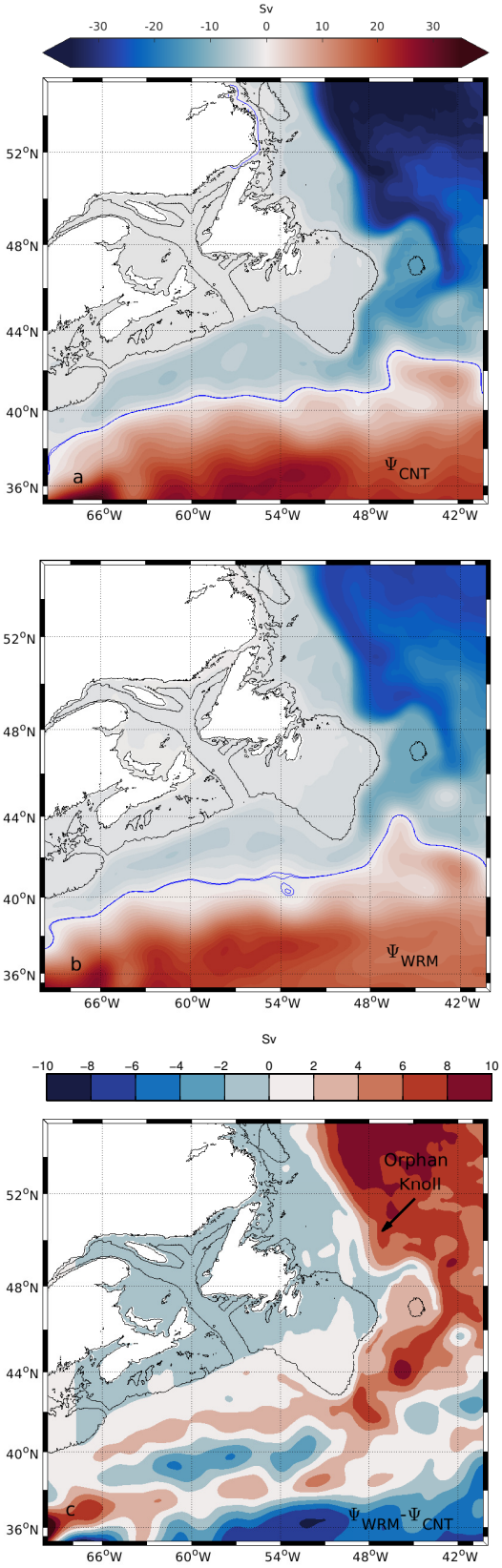

Figure S4. **Labrador Current weakening and impingement of the North Atlantic Current on the Tail of the Grand Banks in model.** Maps of the quasi-streamfunction Ψ, integrated over the upper 1000 m, averaged over the last twenty model years of (a) pre-industrial *control* (CNT) and (b) *warming* (WRM) modeled scenarios. The difference between both scenarios (c) is positive north of 40°N due to weakening of the Labrador Current and northward shift of the Gulf Stream. Between about 36°N and 40°N, the difference is negative due to a slowdown in the Gulf Stream. The 200 m isobath is indicated with a black line and the zero contour with a blue line for reference in (a) and (b). See Methods for details on the computation of Ψ.

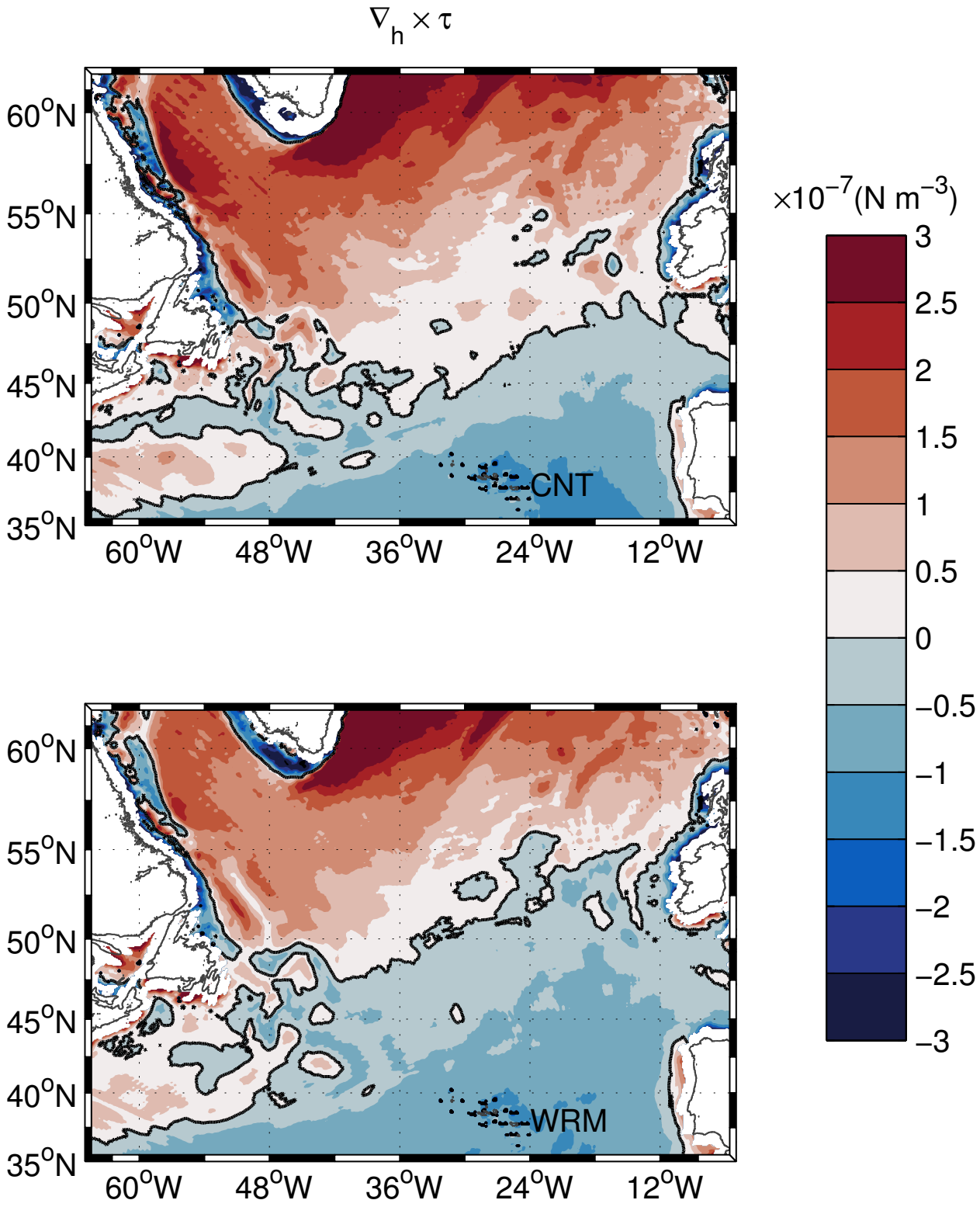

Figure S5. **Modeled weakening of the wind stress curl in the subpolar gyre and poleward shift of its zero line with warming in the North Atlantic**. Wind-stress curl is averaged over the last 20 model years of the pre-industrial *control* (CNT, top) and *warming* (WRM, bottom) scenarios. Zero contour is indicated with a solid black line. See Methods for details on the computation of the wind stress curl.

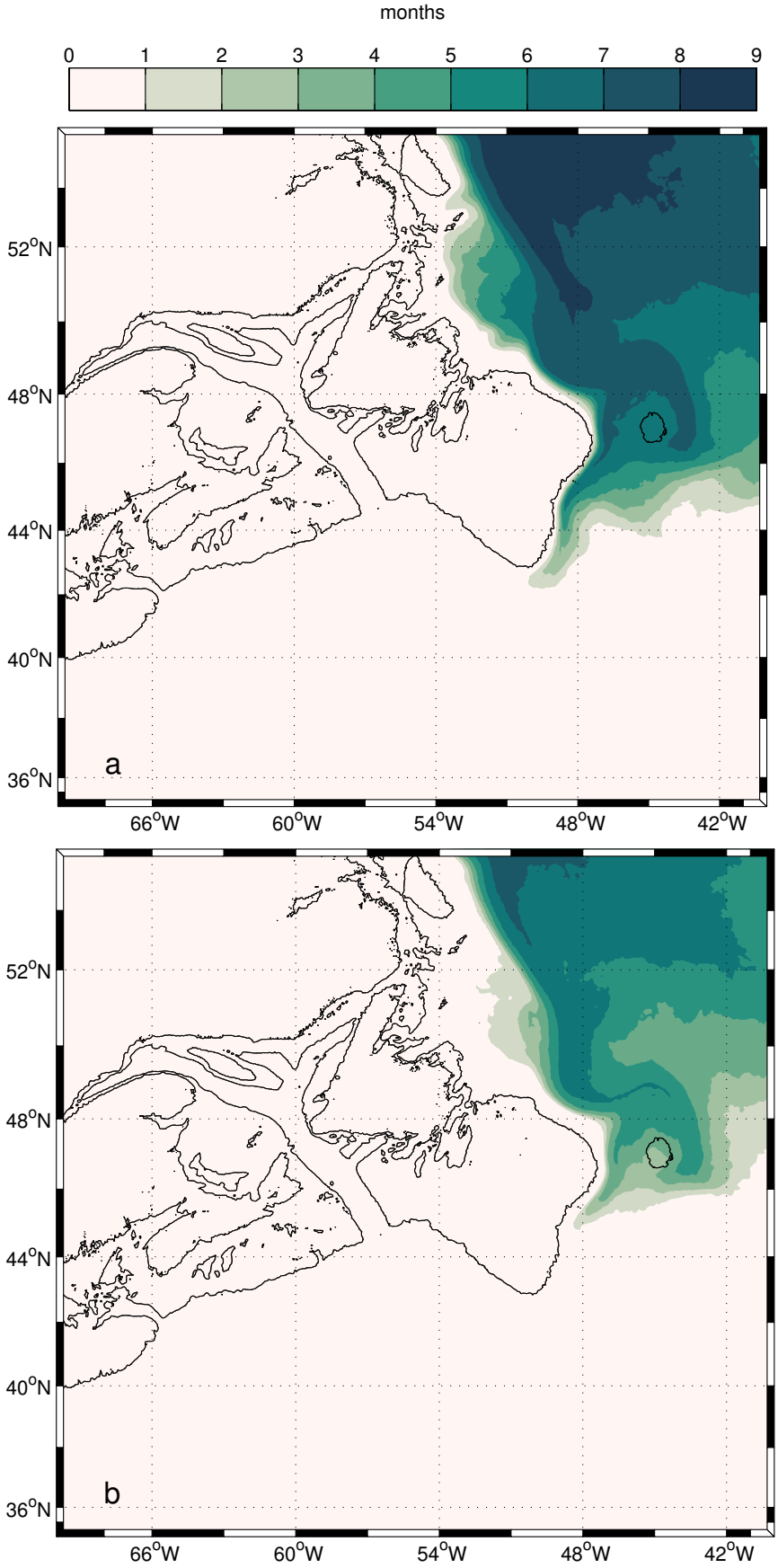

Figure S6. **Reduction of isopycnal outcropping.** Number of months isopycnal $\sigma_\theta = 27.25\,\mathrm{kg\,m^{-3}}$ outcrops averaged over the last twenty model years of (a) pre-industrial *control* and (b) *warming* experiments. The 200 m isobath is indicated with a black line for reference.

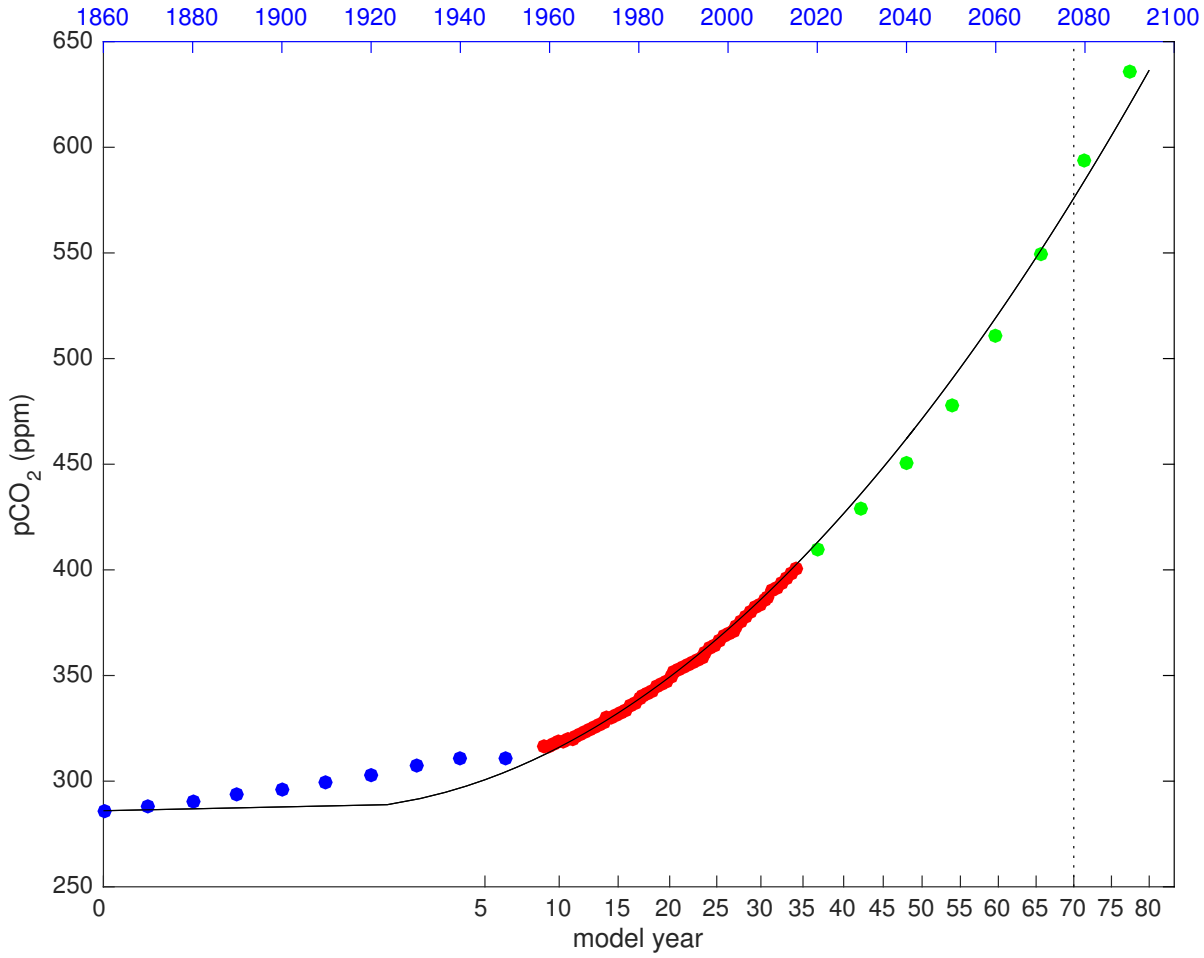

Figure S7. **Time dimension benchmark between CM2.6 model (line) and observations (dots).** Model and observations time dimensions are related through their atmospheric pCO_2. Specifically, the model time dimension is stretched using a polynomial quadratic function that fits to observational/modeled data. Blue dots correspond to CMIP5 recommended preindustrial conditions, red dots to the Mauna Loa Observatory in Hawaii (the so-called Keeling curve, www.esrl.noaa.gov/gmd/ccgg/trends), and green dots to future projections under the RCP6 scenario (https://tntcat.iiasa.ac.at/RcpDb).

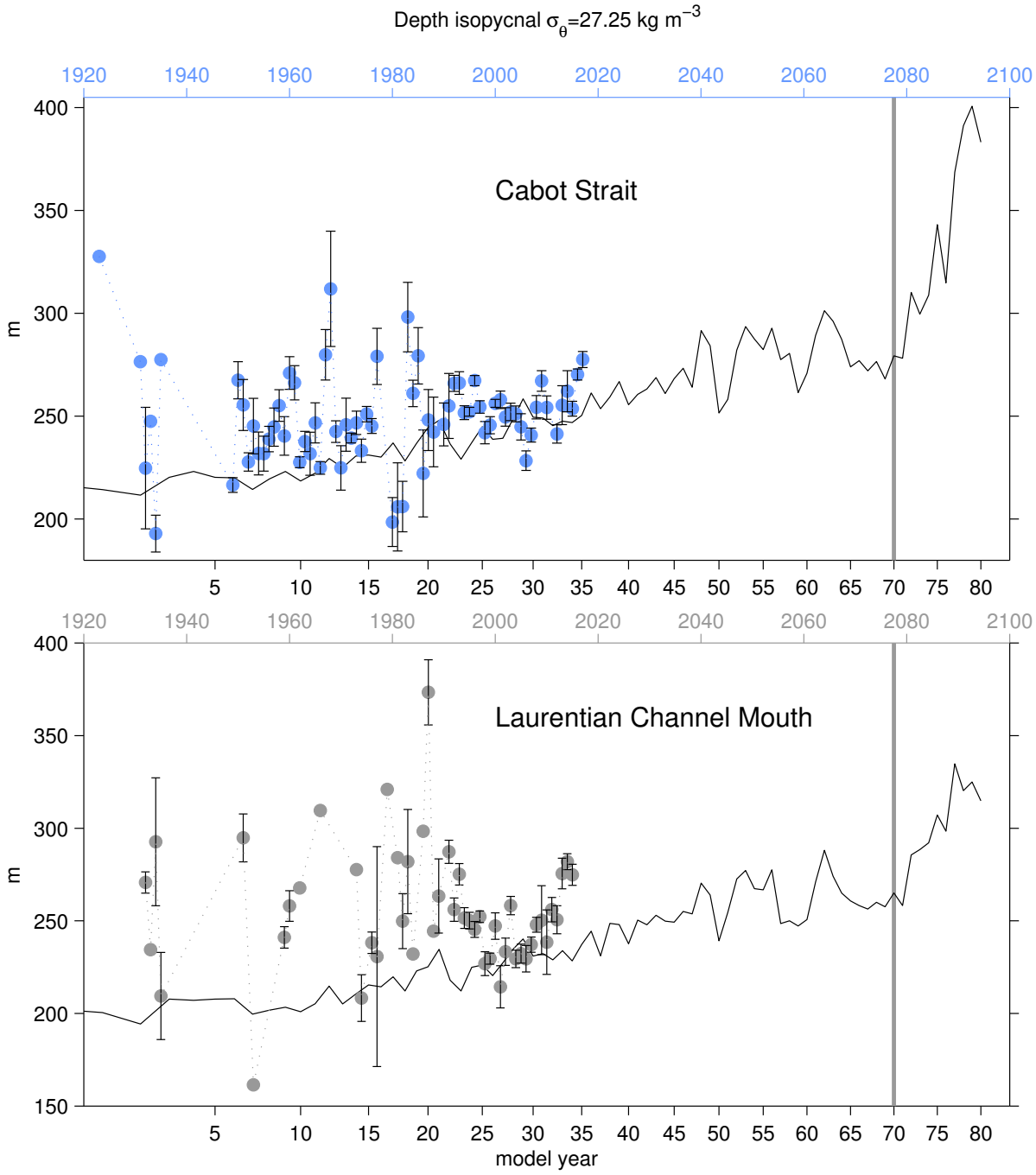

Figure S8. **Observational (dots) and modeled (solid lines) time series of the depth of isopycnal σ_θ = 27.25 kg m^{-3} within the Laurentian Channel.** Same as Figure S1 for the isopycnal depth at Cabot Strait and at the mouth of the Laurentian Channel.

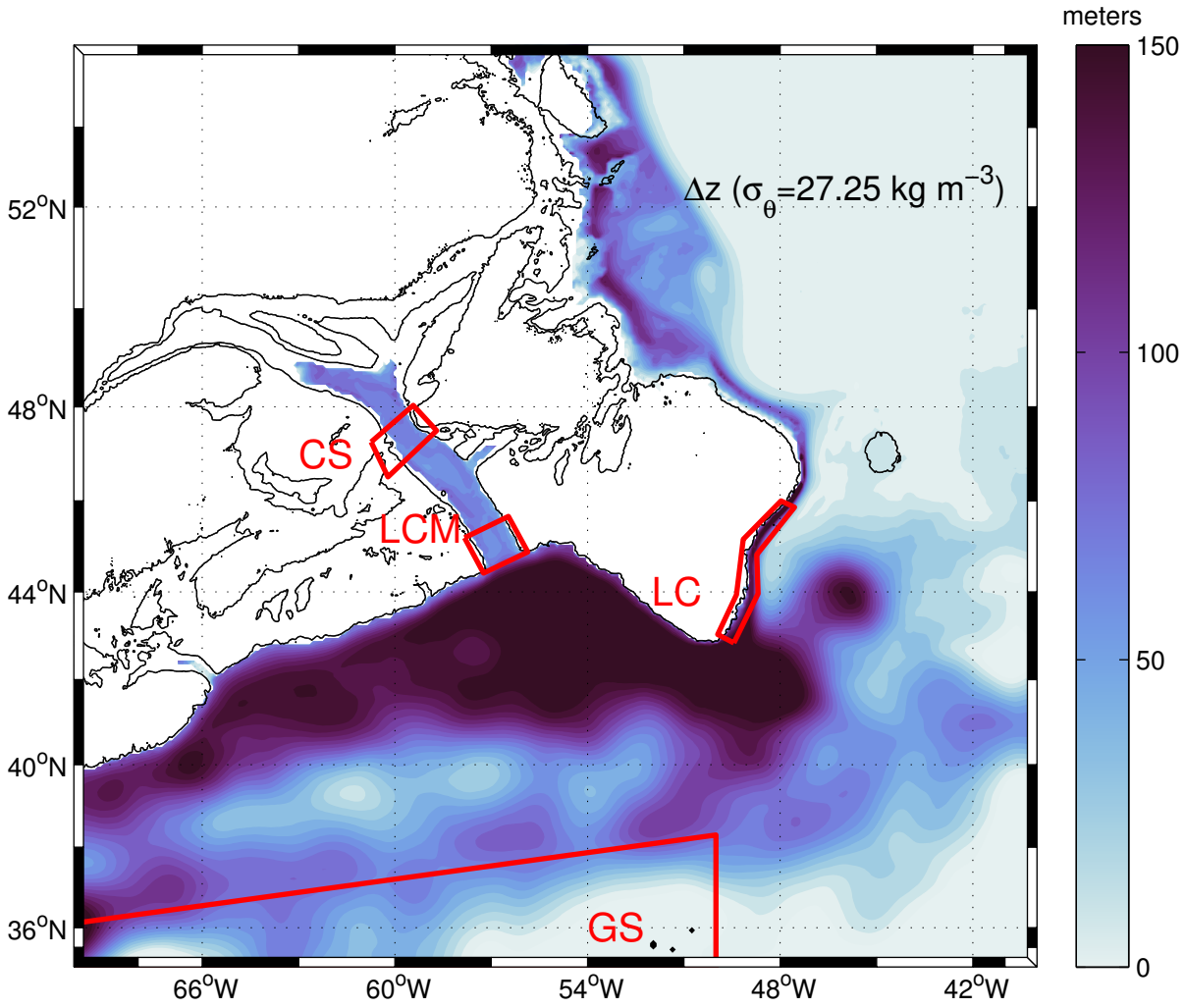

Figure S9. **Modeled deepening of isopycnal $\sigma_\theta = 27.25\,\mathrm{kg\,m^{-3}}$ with idealized warming.** Red boxes indicate regions within the Gulf of St. Lawrence (CS for Cabot Strait and LCM for the Laurentian Channel Mouth) and end member regions (GS for Gulf Stream and LC for Labrador Current). The 200 m isobath is included for reference.

SUPPLEMENTARY TEXT

Decomposition of oxygen changes using mixing model. One can gain further understanding of the simulated changes in oxygen (O_2) by considering the oxygen budget at any point as the sum of the *pre-formed* characteristics of source water masses advected into the region, weighted by their relative contributions, and Apparent Oxygen Utilization (AOU) accumulated along circulation pathways within the region. To this end, a two-end member mixing model (MIX) is constructed for the region with end members chosen to characterize the Gulf Stream (GS) water and the Labrador Current (LC) water immediately northeast of the Tail of the Grand Banks as defined in ref [1] (Fig. S9). The model is applied to an isopycnal surface and considers both oxygen saturation concentration $O_2^{\rm sat}$ and AOU to separate hydrographic effects on O_2 solubility from remineralization processes. Given that AOU is not a conservative tracer, we add a term ($AOU^{\rm path}$) equal to the total remineralization along the path of water mass transport (i.e. that not accounted for by the end member mixing) to obtain

$$\begin{aligned} \mathrm{O_2} &= f\mathrm{O_2^{LC}} + (1-f)\mathrm{O_2^{GS}} - \mathrm{AOU^{path}} \\ &= \underbrace{f\,\mathrm{O_2^{sat,LC}} + (1-f)\,\mathrm{O_2^{sat,GS}}}_{\mathrm{O_2^{sat,MIX}}} \underbrace{-f\,\mathrm{AOU^{LC}} - (1-f)\,\mathrm{AOU^{GS}}}_{-\mathrm{AOU^{MIX}}} - \mathrm{AOU^{path}}, \end{aligned} \tag{1}$$

where f is the fraction of the LC water mass and $1-f$ is that of the GS. These water mass fractions are obtained by solving the following linear system of equations, based on two-end member mixing models for potential temperature referenced at the surface (θ) and salinity (S),

$$\theta = f\,\theta^{\rm LC} + (1-f)\,\theta^{\rm GS}$$

$$\mathrm{S} = f\,\mathrm{S^{LC}} + (1-f)\,\mathrm{S^{GS}},$$

using a least squares fit. End member properties averaged over the last two decades of the climate model are shown in Table S1. The AOU of end members is computed as the modeled difference between $O_2^{\rm sat}$ and O_2. The $AOU^{\rm path}$ is computed as the average of differences between the phosphate concentration (PO_4)

of one end member and that at the location where the mixing model is applied. Phosphate differences are calculated on isopycnals and weighted by the water mass fraction of the corresponding end member. This weighted-averaged phosphate difference is then multiplied by the oxygen to phosphate ratio O_2:P=-150, that is,

$$\mathrm{AOU}^{\mathrm{path}} = -150\left\{f(\mathrm{PO}_4^{\mathrm{LC}} - \mathrm{PO}_4) + (1-f)(\mathrm{PO}_4^{\mathrm{GS}} - \mathrm{PO}_4)\right\}. \tag{2}$$

In order to examine the downstream effects of changes in the LC fraction, we take the Laurentian Channel Mouth site as an example and use averaged values over the last twenty model years. Here, as shown in Table S2, the Labrador Current water mass fraction is halved, decreasing $\mathrm{O}_2^{\mathrm{sat,MIX}}$ and raising *pre-formed* AOU ($\mathrm{AOU}^{\mathrm{MIX}}$) for a total *pre-formed* oxygen decrease of 54 $\mu\mathrm{mol\,kg}^{-1}$. In the model, but not in nature (see Fig. 2), there is a large decline in the AOU accumulated along the circulation pathway ($\mathrm{AOU}^{\mathrm{path}}$) which counteracts more than half of the end-member- and mixing-driven O_2 decrease. Since the isopycnal does not outcrop west of the Grand Banks (Fig. S6), the decrease of AOU must reflect a decrease in the cumulative consumption of oxygen. The decreased oxygen consumption in the model could be attributed to a reduced residence time of waters in the region and/or a reduced rate of oxygen consumption, the latter of which arises from decreased export production as the region stratifies, and is exacerbated as a reduced fraction of the total remineralization occurs on this deepening isopycnal surface [2] (Fig. S9).

The results shown in Table S1 also reveal a significant decrease in the oxygen content of the Labrador Current end member in the *warming* case scenario, with saturation oxygen decreasing by 13 $\mu\mathrm{mol\,kg}^{-1}$ and AOU increasing by 15 $\mu\mathrm{mol\,kg}^{-1}$, while the Gulf Stream end member remains more stable given that the isopycnal does not outcrop at this location (the shallowest depth is reached in the *control* case at 540 m), therefore it is not directly influenced by atmospheric forcing. The decrease in $\mathrm{O}_2^{\mathrm{sat}}$ in the LC end member is due to surface warming and an enrichment of subtropical water in the region as the LC retreats, while the AOU increase can be attributed to a reduction of the exposure of the isopycnal at the surface upstream

of the Grand Banks, resulting from enhanced stratification (Fig. S6), which cuts off the oxygen supply to the isopycnal at its source. To quantify the relevance of LC end member oxygen changes with warming to deoxygenation at the Laurentian Channel Mouth, we next quantify its contribution and compare it with that due to changes in the proportion of water masses.

The oxygen change can be decomposed in terms of end member changes as follows. Defining the change between warming (WRM) and control (CNT) cases as $\Delta \mathrm{O}_2 = \mathrm{O}_2(\mathrm{WRM}) - \mathrm{O}_2(\mathrm{CNT})$ and considering the oxygen decomposition into $\mathrm{O}_2^{\mathrm{sat,MIX}}$, $\mathrm{AOU}^{\mathrm{MIX}}$, and $\mathrm{AOU}^{\mathrm{path}}$, applying the finite difference operator Δ to equation (1) gives

$$\Delta \mathrm{O}_2 = \Delta \mathrm{O}_2^{\mathrm{sat,MIX}} - \Delta \mathrm{AOU}^{\mathrm{MIX}} - \Delta \mathrm{AOU}^{\mathrm{path}}. \tag{3}$$

After applying the product rule of forward differences, changes in $\mathrm{O}_2^{\mathrm{sat,MIX}}$ and $\mathrm{AOU}^{\mathrm{MIX}}$ can be expressed as

$$\begin{aligned} \Delta \mathrm{O}_2^{\mathrm{sat,MIX}} &= \underbrace{\Delta f \left[\mathrm{O}_2^{\mathrm{sat,LC}}(\mathrm{CNT}) - \mathrm{O}_2^{\mathrm{sat,GS}}(\mathrm{CNT})\right]}_{\text{transport}} \\ &+ \underbrace{f(\mathrm{CNT}) \left[\Delta \mathrm{O}_2^{\mathrm{sat,LC}} - \Delta \mathrm{O}_2^{\mathrm{sat,GS}}\right] + \Delta \mathrm{O}_2^{\mathrm{sat,GS}}}_{\text{endmember}} \\ &+ \underbrace{\Delta f \left[\Delta \mathrm{O}_2^{\mathrm{sat,LC}} - \Delta \mathrm{O}_2^{\mathrm{sat,GS}}\right]}_{\text{nonlinear}}, \end{aligned} \tag{4}$$

$$\begin{aligned} \Delta \mathrm{AOU}^{\mathrm{MIX}} &= \underbrace{\Delta f \left[\mathrm{AOU}^{\mathrm{LC}}(\mathrm{CNT}) - \mathrm{AOU}^{\mathrm{GS}}(\mathrm{CNT})\right]}_{\text{transport}} \\ &+ \underbrace{f(\mathrm{CNT}) \left[\Delta \mathrm{AOU}^{\mathrm{LC}} - \Delta \mathrm{AOU}^{\mathrm{GS}}\right] + \Delta \mathrm{AOU}^{\mathrm{GS}}}_{\text{endmember}} \\ &+ \underbrace{\Delta f \left[\Delta \mathrm{AOU}^{\mathrm{LC}} - \Delta \mathrm{AOU}^{\mathrm{GS}}\right]}_{\text{nonlinear}}. \end{aligned} \tag{5}$$

In the above equations, terms involving changes in the fraction of water masses Δf are driven by changes in transport and terms involving changes of the end members are driven by changes in ventilation for AOU and warming for $\mathrm{O}_2^{\mathrm{sat}}$.

The above decomposition of O_2 changes works well at the Laurentian Channel Mouth as shown in

Table S3. The sum of terms in equations (4,5) is in agreement with changes directly computed using the two-end member mixing model (Tables S1, S2). The largest decline in O_2^{sat} and AOU is explained by the transport term, representing a fraction of about 2/3 of the terms contributing to O_2 loss, due to a reduction of the Labrador Current Water transport west of the Tail of the Grand Banks. The remaining fraction of the O_2 decline is explained by changes in the LC end member (endmember and nonlinear terms) associated with warming (decline in $O_2^{sat,LC}$) and a reduction in ventilation (increase in AOU^{LC}). Therefore, property changes in the subpolar end member are non-neglible and should be taken into account when constructing O_2 mixing models in this region.

1. Gilbert, D., Sundby, B., Gobeil, C., Mucci, A. & Tremblay, G.-H. A seventy-two-year record of diminishing deep-water oxygen in the St. Lawrence estuary: The northwest Atlantic connection. *Limnology and Oceanography* **50**, 1654–1666 (2005).

2. Deutsch, C., Brix, H., Ito T., Frenzel H. & Thompson L. Climate-Forced Variability of Ocean Hypoxia *Science* **333**, 336–339 (2011).

SUPPLEMENTARY TABLES

	End member compositions							
	Labrador Current				Gulf Stream			
	θ^{LC}	S^{LC}	$\mathrm{O}_2^{\mathrm{sat,LC}}$	$-\mathrm{AOU}^{\mathrm{LC}}$	θ^{GS}	S^{GS}	$\mathrm{O}_2^{\mathrm{sat,GS}}$	$-\mathrm{AOU}^{\mathrm{GS}}$
CNT	2.6	34.19	328	-41	10	35.39	274	-80
WRM	4.2	34.35	315	-56	9.9	35.37	275	-75
Δ	1.6	0.16	-13	-15	-0.1	-0.02	1	5

Table S1. Changes at the Labrador Current (LC) and Gulf Stream (GS) end member locations of potential temperature (θ in °C), salinity (S), saturation oxygen concentrations ($\mathrm{O}_2^{\mathrm{sat}}$) and Apparent Oxygen Utilization (AOU), both in $\mu\mathrm{mol\,kg}^{-1}$, are shown. All values are averaged over the last twenty years of the pre-industrial *control* (CNT) and *warming* (WRM) climate model scenarios, on the $\sigma_\theta = 27.25\,\mathrm{kg\,m}^{-3}$ isopycnal or at the surface where isopycnal outcrops. Changes (Δ) are computed relative to the pre-industrial *control*, that is, Δ=WRM-CNT for any given property.

	Laurentian Channel Mouth						
	f^{LC}	O_2	O_2^{sat}	$-AOU$	$O_2^{sat,MIX}$	$-AOU^{MIX}$	$-AOU^{path}$
CNT	0.86	219	319	-100	320	-46	-57
WRM	0.34	197	287	-90	288	-68	-18
Δ	-0.52	-22	-32	10	-32	-22	39

Table S2. As in Table S1 but at the Laurentian Channel Mouth (LCM) location. Also shown, are the fraction of Labrador Current water (f^{LC}) and the decomposition of oxygen concentrations following $O_2 = O_2^{sat} - AOU = O_2^{sat,MIX} - AOU^{MIX} - AOU^{path}$, where $O_2^{sat,MIX}$ and AOU^{MIX} are the mixing product of the *pre-formed* end member characteristics, weighted by their proportional contributions as given by f^{LC}. The property AOU^{path} is the AOU accumulated along the pathway from the end members to the LCM site. This simple two end member model works particularly well in this region for O_2^{sat} as shown by the agreement between changes in $O_2^{sat,MIX}$ and changes in the actual O_2^{sat}. Oxygen units are $\mu mol\,kg^{-1}$.

	transport	endmember	nonlinear	SUM
$\Delta O_2^{sat,MIX}$	-28	-11	7	**-32**
$-\Delta AOU^{MIX}$	-20	-12	10	**-22**

Table S3. Changes in O_2^{sat} and AOU at the Laurentian Channel Mouth along isopycnal $\sigma_\theta = 27.25\,kg\,m^{-3}$ decomposed into changes driven by a change in water mass fraction (transport), a change in end member properties (end member), and both (nonlinear). The sum of the three terms (SUM) is in close agreement with changes directly quantified from the mixing model (Table S2). Units are $\mu mol\,kg^{-1}$. All values are averaged over the last twenty years of the pre-industrial *control* and *warming* climate model scenarios.